Science and Technology Indonesia
e-ISSN:2580-4391 *p*-ISSN:2580-4405
Vol. 9, No. 3, July 2024

Research Paper

Removal of Methyl Orange in Aqueous Medium using ZnO/Bentonite as Semiconductor by Photocatalytic Process

Satria Jaya Priatna[1], Ayu Yuliana[2], Zulkarnain[3], Elda Melwita[3], Fitri Suryani Arsyad[4], Risfidian Mohadi[3*]

[1]*Department of Soil Science, Sriwijaya University, Indralaya, South Sumatera, 30862, Indonesia*
[2]*Doctoral Program of Environmental Science, Postgraduate Program, Sriwijaya University, Palembang, South Sumatera, 30139, Indonesia*
[3]*Magister Program of Material Science, Graduate School of Sriwijaya University, Palembang, South Sumatera, 30139, Indonesia*
[4]*Department of Physics, Faculty of Mathematical and Natural Sciences, Sriwijaya University, Indralaya, South Sumatera, 30862, Indonesia*
***Corresponding author**: risfidian.mohadi@unsri.ac.id

Abstract
Pillarization of bentonites (from East Java) with ZnO semiconductors has been synthesized using co-precipitation methods into a ZnO/Bentonite composite and applied as a catalyst in a photocatalytic process to remove Methyl Orange (MO) dyes. The optimum pH condition of MO dyes is at pH 2 with a degradation rate of 22.91% (from 15 mg/L to 11.523 mg/L). The optimum ZnO/Bentonite catalyst weight condition is 200 mg, with a degradation rate of 29.11% (from 15 mg/L to 10.596 mg/L). The optimum time condition for UV lamp irradiation is 60 minutes, with a degradation rate of 64.92% (from 15 mg/L to 5.244 mg/L). The kinetics of MO photocatalytic reaction using ZnO/Bentonite catalyst follows the pseudo-first-order Langmuir-Hinshelwood-Santosa kinetic model with photocatalytic reaction rate constant (k_1) of 0.014 and photocatalytic equilibrium constant (K) of 0.012.

Keywords
ZnO, Bentonite, Methyl Orange, Photocatalytic, Degradation

Received: 26 September 2023, Accepted: 4 April 2024
https://doi.org/10.26554/sti.2024.9.3.539-545

1. INTRODUCTION

MO dyes are included in the waste dyes that are usually produced by the textile industry, and they are dangerous if in high concentrations (Patel and Vashi, 2012). Dyes can cause eye irritation, and skin allergies, and disrupt the human reproductive system if touched and consumed (Shaban et al., 2017). Many technologies have been developed to reduce dye concentrations in wastewater (Shaban et al., 2018). Such methods as adsorption, coagulation-flocculation, and photocatalysis are currently being developed (Fu et al., 2020; Huang et al., 2020; Soliman and Moustafa, 2020). Photocatalysis is considered a better process because the dye will be degraded first by UV light, which can generate hydroxyl radicals as an oxidizer (Ameta et al., 2018). Photocatalytic is a sustainable and inexpensive waste degradation process (Ameta and Prajapati, 2016).

The process of photocatalysis requires a catalyst, which is a semiconductor material. Semiconductor catalysts are the safest materials because their physical or chemical properties remain unchanged during the photocatalytic process (Harun et al., 2018). The semiconductors that are often used to reduce dangerous organic compounds are TiO_2 (band gap: 3.2 eV) and ZnO (band gap: 3.3 eV) because they have high activity, good chemical stability, and are non-toxic (Al-Baghdadi et al., 2022; Nhu et al., 2017).

To increase the degradation percentage, ZnO can be modified with mineral clays that have a high surface area using the pillarization method. Bentonite is one of the good clay minerals to be used as a pillaring agent for semiconductors. The bentonite surface structure consists of three layers of aluminasilicate, where two layers of silica (tetrahedral) bind one layer of alumina (octahedral), and it's stabilized by metal cations Na^{2+}, Ca^{2+}, Mg^{2+}, Fe^{2+}, etc. in the interlayer of bentonite (Özcan et al., 2007). Metal cations can be substituted with metal oxides such as ZnO, TiO_2, and SnO_2 semiconductors using the pillarization method to produce pillared bentonite with a higher surface area and can be used as a catalyst due to the presence of metal oxides (Supeno et al., 2018).

ZnO/Bentonite nanocomposite has been synthesized and reduced the ZnO band gap from 3.3 eV to 3.21 eV, and it's used as a catalyst in phenol and metal Cr(VI) degradation (Chakraborty et al., 2019). SnO_2/Bentonite nanocomposite has been synthesized, where the band gap of SnO_2 has decreased from 3.41 eV to 1.51 eV, and it's used for the degradation of methylene blue, MO, and malachite green (Babu and Antony, 2019). Both of these research studies provide the same

result, which indicates the ZnO-Bentonite or SnO_2/Bentonite catalyst gives a higher degradation percentage than the ZnO or SnO_2 catalyst alone (Babu and Antony, 2019; Chakraborty et al., 2019).

Based on the explanation above, in this research study, pillarization of bentonite with a ZnO semiconductor was synthesized by the co-precipitation method, and the success of synthesis was characterized by X-Ray Fluorescence (XRF), X-Ray Diffraction (XRD), and Diffuse Reflectance/UV-Visible Spectroscopy (DR/UV-Vis). The bentonite used in this study comes from Pacitan (Eastern Java) because it contains Al compounds that affect the closure power of bentonite and contains a Si compound that can absorb organic matter, thus enabling it to be actified, modified, and applied as a catalyst for organic substances such as dyes. ZnO/Bentonite was applied as a catalyst for MO dye photocatalysis. The studied photocatalytic processes are variations in pH dyes, catalyst weight, and UV lamp contact time. The photocatalytic kinetics studied are the pseudo-first-order Langmuir-Hinshelwood kinetic model and the pseudo-second-order Ho-McKay kinetic model. Not only that, in this study, the photocatalytic kinetics were also studied using the derivatives of the Langmuir-Hinshelwood-Santosa formula. In this study, the efficiency of ZnO/Bentonite synthesized from ZnO semiconductors with positive charge surfaces has been modified with bentonites with negative charge surfaces and positive charge interlayers when degraded MO as an anionic dye is well studied.

2. EXPERIMENTAL SECTION

2.1 Chemical and Instrument

The bentonite used was prepared from clay from East Java. Additional chemicals, such as H_2SO_4 97% (Merck), $Zn(NO_3)_2.4H_2O$ (Smart-Lab A-3386 PA/AR), ethanol (Merck), NaOH (Merck), and MO dye. The materials were characterized using several instruments, such as XRF (ARL 9900 series), XRD (Rigaku Miniflex-600), DR/UV-Vis (JASCO V-760), UV-Visible Spectrophotometry (Hitachi U-2900), and 3 pcs of UV-C Lamp (Krisbow 500 Watt, 253.7 nm Wavelength).

2.2 Actifation of Bentonite

Bentonite from East Java was actified using 50 mL of H_2SO_4 with concentrations of 15% for 30 minutes and dried at 110°C. The actified bentonite was characterized using XRF and XRD.

2.3 Synthesis of ZnO/Bentonite

100 mL of 0.05 M $Zn(NO_3)_2.4H_2O$ solution was slowly dosed with NaOH (prepared with ethanol solvent) at 2 M to pH 12 (Romadhan et al., 2016). The reaction was maintained at 70°C for 5 hours. Then, the solution was cooled to a normal temperature and filtered. The ZnO precipitate was dried at 150°C for 3 hours. The synthesized ZnO material of 2 g was reacted into 1 g of actified bentonite dissolved in 250 mL of distilled water, the reaction was maintained at pH 12 and a temperature of 70°C for 5 hours. Then, the ZnO/Bentonite solid was calcinated at 150°C for 4 hours and characterized using XRD and DR/UV-VIS.

2.4 Photocatalytic Method

2.4.1 Variation of MO pH

200 mg of ZnO/Bentonite was reacted with 20 mL of MO 15 mg/L solution for 20 minutes at pH 2; 3.5; 6.

2.4.2 Variation of ZnO/Bentonite Weigh

20 mL of MO 15 mg/L was reacted with 100, 200, 300, 400, and 500 mg ZnO/Bentonite for 20 minutes at optimum pH conditions.

2.4.3 Variation of UV Lamp Irradiation Time

20 mL of MO 15 mg/L was reacted with ZnO/Bentonite under conditions of optimum pH of MO and optimum weight of ZnO/Bentonite exposed to UV light for 10, 20, 30, 40, 50, 60, 70, and 80 minutes.

All photocatalytic processes were worked on a closed box illuminated by three UV-C lamps on the top, left, and right. In this removal, MO with a photocatalytic process, the variation of MO pH, variation of ZnO/Bentonite weigh, and variation of UV lamp irradiance time will be studied. The percentage of degradation MO will be calculated using the following Equation 1.

$$\%\text{Degradation} = \left(\frac{C_0 - C_t}{C_0}\right) \times 100\% \quad (1)$$

C_0 represents the initial concentration of MO and C_t represents the final concentration of MO after the photocatalytic process at time (t) minutes. The photocatalytic kinetics studied were determined using the pseudo-first-order Langmuir-Hinshelwood kinetic model following Equation 2 and the pseudo-second-order Ho kinetic model following Equation 3 (Prandini et al., 2022).

$$\frac{\ln \frac{C_0}{C_t}}{C_0 - C_t} + K = \frac{k_1 \cdot t}{C_0 - C_t} \quad (2)$$

k_1 is the reaction rate constant at pseudo-first-order and K is the photocatalytic equilibrium constant (Langmuir-Hinshelwood kinetic model).

$$\frac{t}{Q_t} = \frac{1}{k_2 \cdot Q_e^2} + \frac{1}{Q_e} t \quad (3)$$

Q_e (mg/g) represents the degradation capacity at equilibrium; Q_t (mg/g) represents the degradation capacity at time (t); and k_2 is the reaction rate constant at pseudo-second-order (Ho-McKay kinetic model). Degradation capacity (Q_t) can be calculated following Equation 4.

$$Q_t = \frac{(C_o - C_e).V}{w} \quad (4)$$

3. RESULTS AND DISCUSSIONS

Natural bentonite actified using H_2SO_4 at 15% causes the bentonite interlayer to swell and the active side to increase (Erliyanti et al., 2020). The results of XRF measurements of actified bentonite are presented in Table 1. The results show the type of bentonite is Ca-bentonite due to the presence of CaO content of 2.35% and the absence of Na_2O.

Table 1. XRF Result of Actifed Bentonite

Composition	Presentation (%)
SiO_2	64.91
Al_2O_3	5.07
Fe_2O_3	2.92
K_2O	0.25
CaO	2.35
MgO	0.44
Na_2O	0.00

In line with these results, the XRD spectrum shows in Figure 1 the characterization of Bentonite modified with ZnO as a semiconductor with a ratio of 2:1 (Bentonite:ZnO). A typical bentonite peak will appear at 20.7° and quartz at 36.3° (Hebbar et al., 2018). Typical montmorillonite peaks will appear at 2θ 20-22°, 35°, and 68° while quartz peaks appear at 2θ 25-28° (Zaher MS et al., 2018). Typical diffraction peaks of ZnO include 31.7°, 34.3°, 36.3°, 47.5°, 56.7°, 62.9°, and 68.01° (Chakraborty et al., 2019). These peaks indicate the hexagonal crystal planes of ZnO (Muhammad et al., 2019). Peaks 68-70° indicate ZnO produced in the hexagonal wurtzite structure, which is the most stable and cleanest ZnO structure from contaminants (Yedurkar et al., 2016).

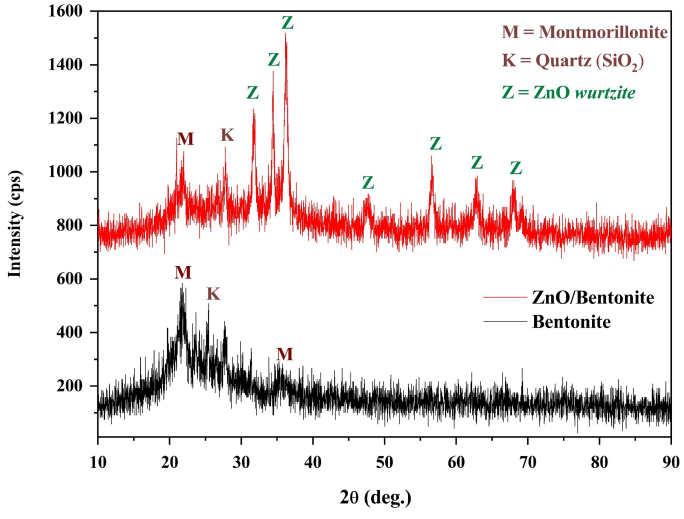

Figure 1. XRD Patterns of Bentonite and ZnO/Bentonite

Figure 1 shows the XRD patterns of the actified bentonite. Peaks 22.02° and 35.46° show typical Ca-Montmorillonite, and peak 23.92° shows quartz (SiO_2) in bentonite. Figure 1 shows the XRD patterns of ZnO/Bentonite. Peaks 31.76°,

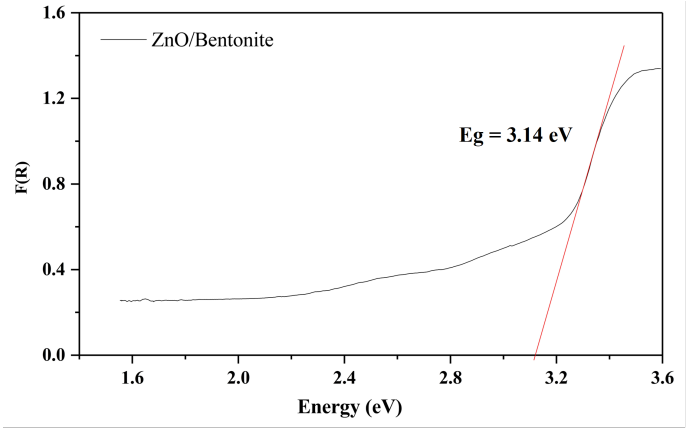

Figure 2. Kubelka-Munk Plot Curve of ZnO/Bentonite

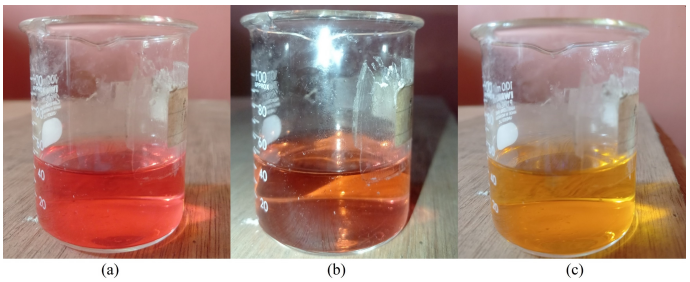

Figure 3. MO Color Conditions at pH 2(a); 3.5(b); 6(c)

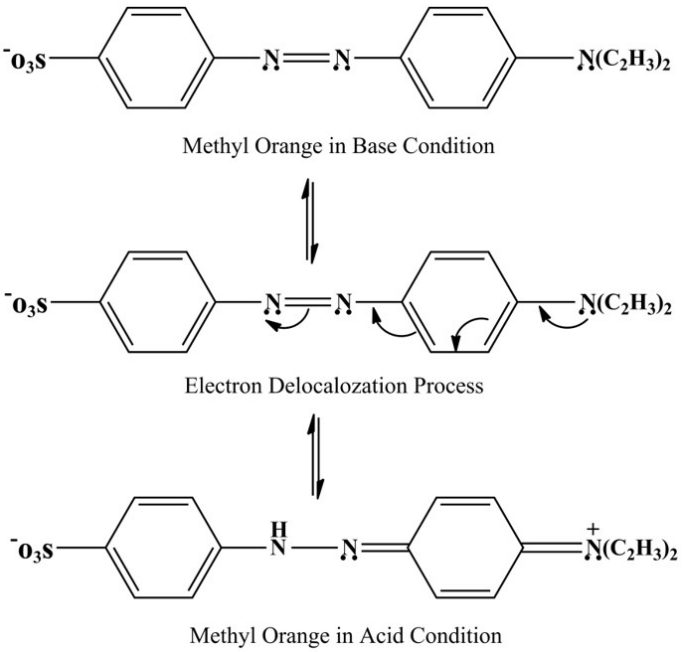

Figure 4. Structure of MO if Delocalized of Electrons in Acid and Base Conditions

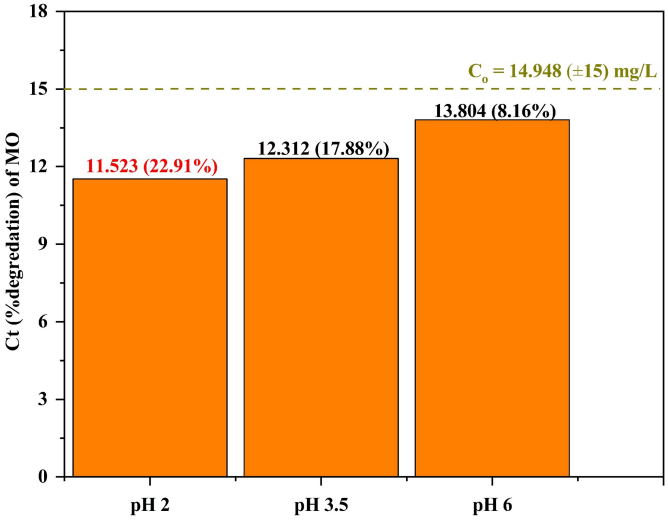

Figure 5. C_t of MO (%Degradation) at Variations of pH MO

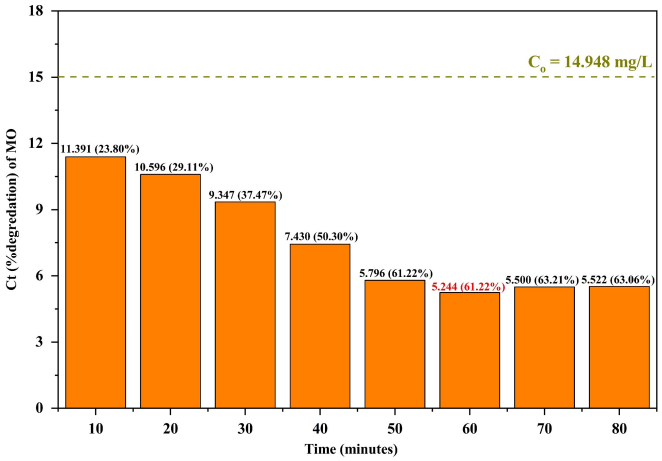

Figure 7. C_t of MO (%Degradation) at Variation of UV Irradiation Time

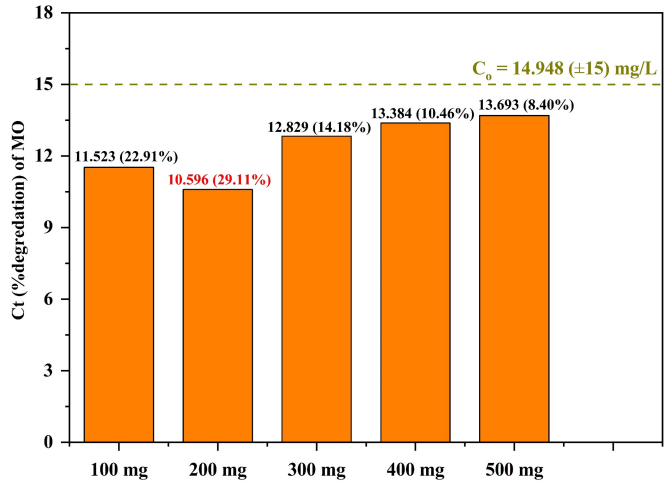

Figure 6. C_t of MO (%Degradation) at Variation of ZnO/Bentonite Weight

34.4°, 36.26°, 47.49°, 56.65°, 62.79°, and 68.03° show the wurtzite hexagonal structure of ZnO. Peak 21.59° shows Ca-Montmorillonite, and peak 27.84° shows quartz of bentonite. Typical bentonite and ZnO peaks appear in the resulting XRD patterns, so it can be said that both were successfully modified (Byun et al., 2023; Khobzaoui et al., 2019).

Peak 22.02° in XRD patterns of bentonite has a d-spacing of 4.032Å. D-spacing shows the interlayer distance of the aluminum silicate structure of bentonite. Then, peak 21.59° in the XRD results of ZnO/Bentonite has a d-spacing of 4.12Å. The values of these two d-spacings don't have a significant difference. It shows that ZnO doesn't enter the interlayer of bentonite, but only attaches to the bentonite surface. This may be because Ca-bentonite is more difficult to swell than Na-bentonite, which makes it difficult for ZnO to enter the bentonite interlayer (Byun et al., 2023). The crystal structure of bentonite is also rigid (Khobzaoui et al., 2019), making it difficult to change its structure, making it difficult for ZnO to attach to the bentonite interlayer and only attach to the surface.

Figure 2 shows the Kubelka-Munk Plot Curve of ZnO/Bentonite. In general, the band gap of ZnO is about 3.2-3.37 eV (Chakraborty et al., 2019; Kumar et al., 2015). Modified ZnO with Bentonite decreases the ZnO band gap to 3.14 eV. If the band gap value is smaller, the energy needed in the electron excitation process when the degradation process occurs is also smaller, so it can increase the percentage of degradation (Pelaez et al., 2012).

The synthesized ZnO/Bentonite was applied as a catalyst (semiconductor) in the MO photocatalytic process. The pH range of MO is 3.1-4.4 (Niu, 2013). So to find the optimum pH conditions for MO photocatalytic, it was applied in 3 conditions, including pH conditions below the pH range of MO at pH 2 when MO is red, pH range conditions of MO at pH 3.5 when MO is orange, and at pH conditions above the pH range of MO at pH 6 when MO is yellow as shown in Figure 3. The maximum wavelength obtained from each pH 2, 3.5, and 6 is 504 nm, 495 nm, and 464 nm.

Figure 4 shows the changes in MO structure at acid and base conditions. The delocalization of electrons in the MO structure will occur when the pH is changed, as shown in Figure 4. When the MO condition is acidic (pH 2), H^+ ions in the MO structure increase, so more conjugated double bonds are formed, which cause a shift at longer wavelengths. This is called a bathochromic shift or red shift. Thus, MO will be more positively charged in acidic conditions (Pratiwi et al., 2020).

The results of MO degradation using a ZnO/Bentonite catalyst are shown in Figure 5. According to Figure 5, Co MO of 14.948 mg/L (±15 mg/L) gave Ct of 11.523 mg/L at pH 2, 12.312 mg/L at pH 3.5, and 13.804 mg/L at pH 6 when degraded by ZnO/Bentonite/UV. These results show that the

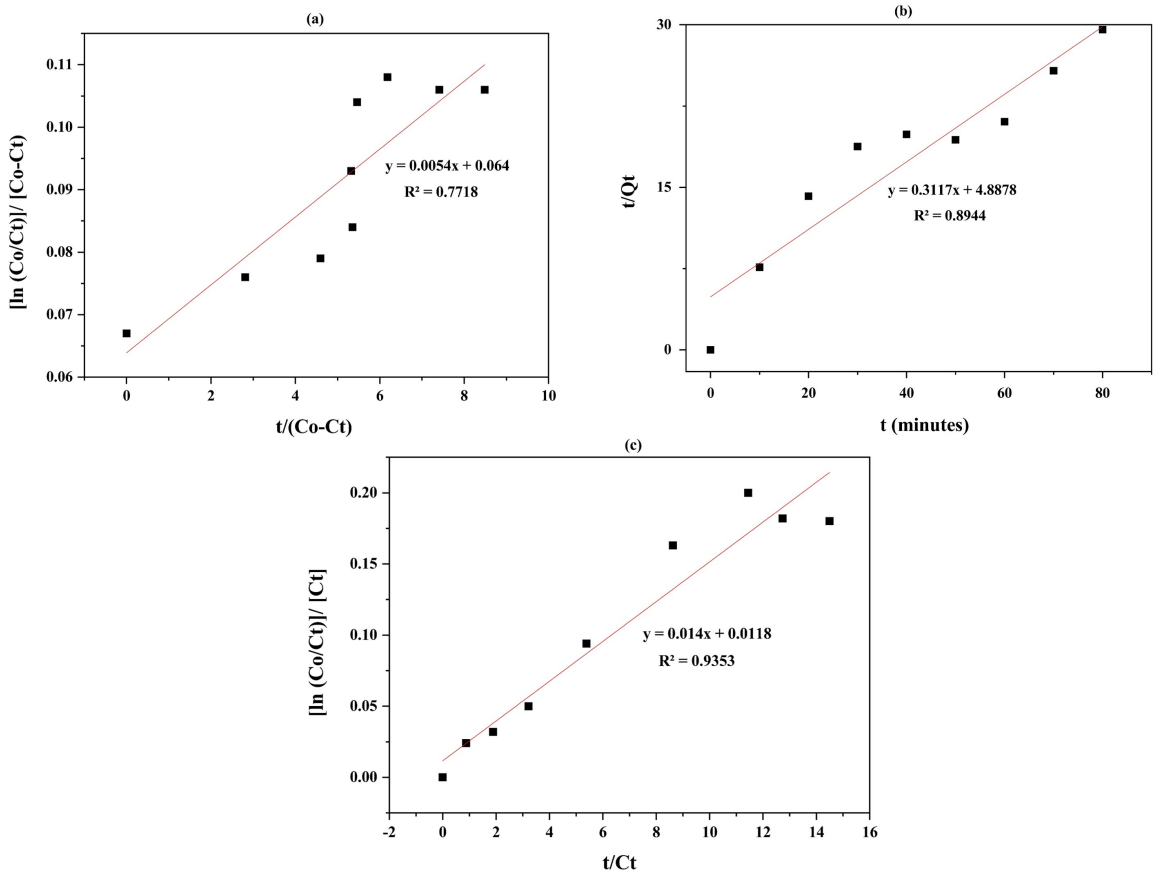

Figure 8. Langmuir-Hinshelwood (a); Ho-McKay (b); Langmuir-Hinshelwood-Santosa (c) Kinetic Curve

highest percent degradation occurred during MO conditions at pH 2 of 22.91%. As explained earlier, at an acidic pH of 2, MO will be positively charged, which makes it easier to attach to the bentonite surface, which is negatively charged (Baik and Lee, 2010) before the degradation process occurs.

Figure 6 shows the Ce and %degradation of MO (15 mg/L) conducted under conditions of ZnO/Bentonite catalyst weight variation and at optimum pH conditions (pH 2). According to Figure 6, ZnO/Bentonite with 200 mg weight degraded MO of 4,404 mg/L (Ct MO = 10,596 mg/L) gave the highest percent degradation result, namely 29.11%. Figure 6 shows that when the weight of ZnO/Bentonite is 300, 400, and 500 mg, the percent degradation is decreased. This is perhaps because when the weight of ZnO/Bentonite is >200 mg, it will cover the MO particles, making it difficult for UV light to degrade the MO dyes.

Based on the above observations, the MO degradation process was continued by varying the UV lamp irradiation time at the optimum pH of MO (pH 2) and the optimum weight of ZnO/Bentonite (200 mg). The results of MO (15 mg/L) degradation based on variations in UV irradiation time are shown in Figure 7. According to Figure 7, the optimum time of MO degradation is 60 minutes, which degraded MO by 9.756 mg/L (Ct MO = 5.244 mg/L) and showed the highest percent degradation of 64.92%. Figure 6 shows an increase in the percent degradation of MO from 10 minutes to 60 minutes but a not-so-significant decrease in percent degradation at 70 and 80 minutes. At this time, the percent degradation shows an equilibrium condition. If the UV irradiation time is increased, the percent degradation can decrease continuously. This is possible because if the degradation of MO by ZnO/Bentonite is longer, ZnO/Bentonite is in a saturated condition to degrade MO, which can cause MO to be released from the catalyst surface and the percent degradation will decrease.

Based on the UV irradiation time data above, the pseudo-first-order Langmuir-Hinshelwood kinetic model (Equation 2) and the pseudo-second-order Ho kinetic model (Equation 3) were studied. The kinetic model calculation data is shown in Table 2.

Based on Equation 2 and Table 2. the Langmuir-Hinshelwo od kinetic curve is shown in Figure 8(a). k_1 (reaction rate constant) of pseudo-first order is indicated by the slope value. and K (photocatalytic equilibrium constant) is indicated by the intercept value. Based on Equation 3 and Table 2. the Ho-McKay kinetic curve is shown in Figure 8(b). k_2 (reaction rate constant) of pseudo-second order is indicated by intercept and $\frac{1}{k_2 \cdot Q_e^2}$. The reaction constants and linear regression values are shown in Table 3.

Table 2. Langmuir-Hinshelwood Kinetic Model Calculation

Time (Minutes)	C_t (mg/L)	$C_o - C_t$ (mg/L)	$\frac{t}{C_o - C_t}$	$\frac{C_o}{C_t}$	$\ln \frac{C_o}{C_t}$	$\frac{\ln \frac{C_o}{C_t}}{C_o - C_t}$	$\frac{t}{C_t}$	$\frac{\ln \frac{C_o}{C_t}}{C_t}$	Q_t	$\frac{t}{Q_t}$
0	14.948	0.000	0.000	1.000	0.000	0.067	0.000	0.000	1.000	0.000
10	11.391	3.557	2.811	1.312	0.272	0.076	0.878	0.024	1.312	7.620
20	10.596	4.352	4.596	1.411	0.344	0.079	1.888	0.032	1.411	14.177
30	9.347	5.601	5.356	1.599	0.469	0.084	3.210	0.050	1.599	18.759
40	7.430	7.518	5.320	2.012	0.699	0.093	5.384	0.094	2.012	19.882
50	5.796	9.152	5.463	2.579	0.947	0.104	8.626	0.163	2.579	19.388
60	5.244	9.704	6.183	2.850	1.047	0.108	11.441	0.200	2.850	21.051
70	5.500	9.448	7.409	2.718	1.000	0.106	12.728	0.182	2.718	25.755
80	5.522	9.426	8.487	2.707	0.996	0.106	14.488	0.180	2.707	29.553

Table 3. Calculation of Kinetics Model of MO Photocatalytic

Kinetic Model	Parameters	Value
Langmuir-Hinshelwood	R^2	0.772
	k_1	0.005
	K	-0.064
Ho-McKay	R^2	0.894
	k_2	0.064
Langmuir-Hinshelwood- Santosa	R^2	0.935
	k_1	0.014
	K	0.012

According to Table 3, the value of K in kinetics is negative. In thermodynamics. the value of the reaction constant is not allowed to be negative. Langmuir-Hinshelwood kinetics are refined (Santosa et al., 2007) and the initial concentration (C_0) doesn't affect the reaction rate in the photocatalytic process. so it is recalculated using Langmuir-Hinshelwood-Santosa kinetics using the following formula Equation 5.

$$\frac{\ln \frac{C_0}{C_t}}{C_t} = \frac{k_1 \cdot t}{C_t} + K \tag{5}$$

4. CONCLUSIONS

Bentonite from East Java has been successfully modified with a ZnO semiconductor (band gap: 3.14 eV) and applied as a catalyst in the photocatalytic process to remove MO dye concentration. The success of ZnO/Bentonite material modification was characterized using XRF. XRD. and DR/UV-Vis. In the photocatalytic process that has been carried out. the optimum pH for MO dye degradation is pH 2. the optimum weight of the ZnO/Bentonite catalyst is 200 mg. and the optimum time of UV lamp irradiation is 60 minutes. The kinetics of MO photocatalytic reaction using ZnO/Bentonite catalysts follow the pseudo-first-order Langmuir-Hinshelwood-Santosa kinetics model with a photocatalytic reaction rate constant (k_1) of 0.014 and a photocatalytic equilibrium constant (K) of 0.012. The ZnO/Bentonite composite's catalyst degradation capabilities are quite good in this study. ZnO semiconductors with positive charge surfaces have been modified with bentonites with negative charge surfaces and positive charge interlayers. capable of degrading MO dye up to 64.92%.

5. ACKNOWLEDGMENT

The research/publication of this article was funded by DIPA of Public Service Agency of Universitas Sriwijaya 2023. SP DIPA-23.17.2.677515/2023. On November 13. 2022. In accordance with the Rector's Decree Number: 0188/UN9.3.1/SK/2023. On April 18. 2023.

REFERENCES

Al-Baghdadi, S. B., H. I. Abdullah, and A. A. Al-Amiery (2022). Synthesis of ZnO Nanoparticles for Photodegradation of Clofibrate Acid as Organic Pollutant. *International Journal of Health Sciences*, **6**(4); 3124–3131

Ameta, R. and D. I. Prajapati (2016). Synthesis, Characterization and Application of Nano-Sized Barium Chromate for Degradation of Erythrosine B. In *Indonesian Journal of Chemistry*, volume 14

Ameta, R., M. S. Solanki, S. Benjamin, and S. C. Ameta (2018). Photocatalysis. In *Advanced Oxidation Processes for Wastewater Treatment: Emerging Green Chemical Technology*. Elsevier Inc., pages 135–175

Babu, A. T. and R. Antony (2019). Clay Semiconductor Hetero-System of SnO_2/Bentonite Nanocomposites for Catalytic Degradation of Toxic Organic Wastes. *Applied Clay Science*, **183**(December); 105312

Baik, M. H. and S. Y. Lee (2010). Colloidal Stability of Bentonite Clay Considering Surface Charge Properties as a Function of pH and Ionic Strength. *Journal of Industrial and Engineering Chemistry*, **16**(5); 837–841

Byun, Y., C. Seo, T. Yun, Y. Joo, and H. Young Jo (2023). Prediction of Na- and Ca-Montmorillonite Contents and Swelling Properties of Clay Mixtures Using Vis-NIR Spectroscopy. *Geoderma*, **430**(February); 1–16

Chakraborty, T., A. Chakraborty, M. Shukla, and T. Chat-

topadhyay (2019). ZnO–Bentonite Nanocomposite: An Efficient Catalyst for Discharge of Dyes, Phenol and Cr(VI) from Water. *Journal of Coordination Chemistry*, **72**(1); 53–68

Erliyanti, N. K., S. Muljani, D. Baskoro, and N. W. Erza Prastika (2020). Synthesis and Characterization of Adsorbent from Solid Waste of Ceramics Industry. *Journal of Physics: Conference Series*, **1569**(3); 1–6

Fu, Y., Q. Li, J. Liu, Y. Jiao, S. Hu, H. Wang, S. Xu, and B. Jiang (2020). In-situ Chemical Vapor Deposition to Fabricate Cuprous Oxide/Copper Sulfide Core-Shell Flowers with Boosted and Stable Wide-Spectral Region Photocatalytic Performance. *Journal of Colloid and Interface Science*, **570**; 143–152

Harun, N. H., M. N. A. Rahman, W. F. W. Kamarudin, Z. Irwan, A. Muhammud, N. E. F. M. Akhir, and M. R. Yaafar (2018). Photocatalytic Degradation of Congo Red Dye Based on Titanium Dioxide Using Solar and UV Lamp. *Journal of Fundamental and Applied Sciences*, **10**(1S); 832–846

Hebbar, R. S., A. M. Isloor, B. Prabhu, Inamuddin, A. M. Asiri, and A. F. Ismail (2018). Removal of Metal Ions and Humic Acids Through Polyetherimide Membrane with Grafted Bentonite Clay. *Scientific Reports*, **8**(1); 1–16

Huang, X., Y. Wan, B. Shi, and J. Shi (2020). Effects of Powdered Activated Carbon on the Coagulation-Flocculation Process in Humic Acid and Humic Acid-Kaolin Water Treatment. *Chemosphere*, **238**; 124637

Khobzaoui, S., L. Tennouga, I. K. Benabadji, A. Mansri, and B. Bouras (2019). Preparation of Rigid Bentonite/PAM Nanocomposites by an Adiabatic Process: Influence of Load Content and Nano-Structure on Mechanical Properties and Glass Transition Temperature. *Journal of Inorganic and Organometallic Polymers and Materials*, **29**(4); 1111–1118

Kumar, M., S. Kumar, Z. Parveen, J. Kaur, N. Sharma, and B. Bansod (2015). Facial Synthesis of Nano Sized ZnO by Hydrothermal Method. *International Journal of Advanced Research in Electrical, Electronics and Instrumentation Engineering*, **4**(5); 4440–4444

Muhammad, W., N. Ullah, M. Haroon, and B. H. Abbasi (2019). Optical, Morphological and Biological Analysis of Zinc Oxide Nanoparticles (ZnO NPs) Using: Papaver somniferum L. *RSC Advances*, **9**(51); 29541–29548

Nhu, V. T. T., D. QuangMinh, N. N. Duy, and N. QuocHien (2017). Photocatalytic Degradation of Azo Dye (Methyl Red) In Water under Visible Light Using Ag-Ni/TiO2 Sythesized by Irradiation Method. *International Journal of Environment, Agriculture and Biotechnology*, **2**(1); 529–538

Niu, P. (2013). Photocatalytic Degradation of Methyl Orange in Aqueous TiO2 Suspensions. *Asian Journal of Chemistry*, **25**(2); 1103–1106

Patel, H. and R. T. Vashi (2012). Removal of Congo Red Dye from its Aqueous Solution using Natural Coagulants. *Journal of Saudi Chemical Society*, **16**(2); 131–136

Pelaez, M., N. T. Nolan, S. C. Pillai, M. K. Seery, P. Falaras, A. G. Kontos, P. S. M. Dunlop, J. W. J. Hamilton, J. A. Byrne, K. O'Shea, M. H. Entezari, and D. D. Dionysiou (2012). A Review on the Visible Light Active Titanium Dioxide Photocatalysts for Environmental Applications. In *Applied Catalysis B: Environmental*, volume 125. pages 331–349

Prandini, M. N., Pranoto, and S. D. Marliyana (2022). A Comparative Study of Kinetics of Methylene Blue Dye using Adsorbent Andisol and Humic Acid from Lighnite by KOH-Hydrothermal Method. *Journal of Physics: Conference Series*, **2190**(1)

Pratiwi, S. W., S. N. Sari, R. Nurmalasari, and M. Indriani (2020). Utilization of Nata de Coco as Adsorben in Methyl Orange Adsorption. *EduChemia (Jurnal Kimia Dan Pendidikan)*, **5**(2); 187

Romadhan, M. F., N. E. Suyatma, and F. M. Taqi (2016). Synthesis of ZnO Nanoparticles by Precipitation Method with Their Antibacterial Effect. *Indonesian Journal of Chemistry*, **16**(2); 117–123

Santosa, S. J., D. Siswanta, A. Kurniawan, and W. H. Rahmanto (2007). Hybrid of Chitin and Humic Acid as High Performance Sorbent for Ni(II). *Surface Science*, **601**(22); 5155–5161

Shaban, M., M. R. Abukhadra, A. Hamd, R. R. Amin, and A. Abdel Khalek (2017). Photocatalytic Removal of Congo Red Dye using MCM-48/Ni2O3 Composite Synthesized Based on Silica Gel Extracted from Rice Husk Ash; Fabrication and Application. *Journal of Environmental Management*, **204**; 189–199

Shaban, M., M. I. Sayed, M. G. Shahien, M. R. Abukhadra, and Z. M. Ahmed (2018). Adsorption Behavior of Inorganic- and Organic-Modified Kaolinite for Congo Red Dye from Water, Kinetic Modeling, and Equilibrium Studies. *Journal of Sol-Gel Science and Technology*, **87**(2); 427–441

Soliman, N. K. and A. F. Moustafa (2020). Industrial Solid Waste for Heavy Metals Adsorption Features and Challenges; A Review. *Journal of Materials Research and Technology*, **9**(5); 10235–10253

Supeno, M., N. Pasaribu, and R. Siburian (2018). Role of TiO2 Pillared Bentonite and Catalyst Nickel for Hydrogenation Glucose to Generate Sorbitol. *Oriental Journal of Chemistry*, **34**(6); 2819–2825

Yedurkar, S., C. Maurya, and P. Mahanwar (2016). Biosynthesis of Zinc Oxide Nanoparticles Using Ixora Coccinea Leaf Extract—A Green Approach. *Open Journal of Synthesis Theory and Applications*, **05**(01); 1–14

Zaher MS, A., A. Wahab SM, T. MH, and M. AM (2018). Sorption Characteristics of Iron, Fluoride and Phosphate from Wastewater of Phosphate Fertilizer Plant using Natural Sodium Bentonite. *Journal of Membrane Science & Technology*, **08**(02); 1–10

Özcan, A., C. Ömeroğlu, Y. Erdoğan, and A. S. Özcan (2007). Modification of Bentonite with a Cationic Surfactant: An Adsorption Study of Textile Dye Reactive Blue 19. *Journal of Hazardous Materials*, **140**(1–2); 173–179

